Accepted Manuscript

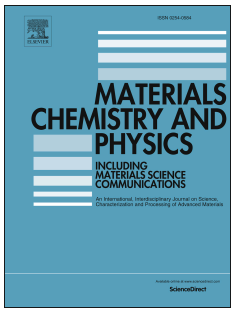

Novel synthesis and properties of hydrogen-free detonation nanodiamond

Stepan S. Batsanov, Alexander N. Osavchuk, Stepan P. Naumov, Sergey M. Gavrilkin, Anatoly S. Leskov, Budhika G. Mendis, Andrew Beeby, Andrei S. Batsanov

PII: S0254-0584(18)30477-2

DOI: 10.1016/j.matchemphys.2018.05.072

Reference: MAC 20687

To appear in: *Materials Chemistry and Physics*

Received Date: 28 May 2017

Revised Date: 25 April 2018

Accepted Date: 28 May 2018

Please cite this article as: S.S. Batsanov, A.N. Osavchuk, S.P. Naumov, S.M. Gavrilkin, A.S. Leskov, B.G. Mendis, A. Beeby, A.S. Batsanov, Novel synthesis and properties of hydrogen-free detonation nanodiamond, *Materials Chemistry and Physics* (2018), doi: 10.1016/j.matchemphys.2018.05.072.

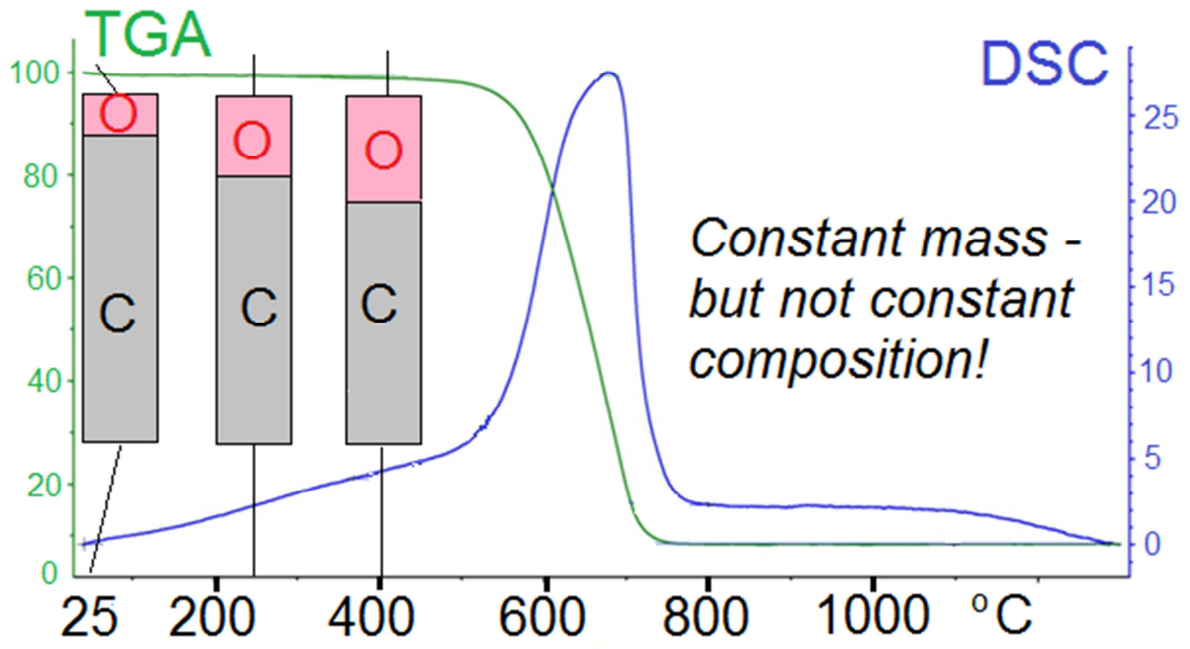

Novel synthesis and properties of hydrogen-free detonation nanodiamond

Stepan S. Batsanov,[a,*] Alexander N. Osavchuk,[b] Stepan P. Naumov,[b] Sergey M. Gavrilkin,[a] Anatoly S. Leskov,[a] Budhika G. Mendis,[c] Andrew Beeby[d] and Andrei S. Batsanov[d]

[a]*National Research Institute of Physical-Technical Measurements, Moscow Region, 141570, Russia*

[b]*Federal State Unitary Enterprise Soyuz, Moscow Region, 140090, Russia*

[c]*Physics Department, Durham University, Science Site, South Road, DH1 3LE, UK*

[d]*Chemistry Department, Durham University, Science Site, South Road, DH1 3LE, UK*

Abstract

Practically hydrogen-free nanodiamond (HFND), a prospective neutron-optical material, was prepared (in up to 3% yield) by detonating pure or graphite-doped RDX in an ice shell and comprehensively characterized by elemental analysis, X-ray diffraction, TEM, SAED, EELS, Raman and IR spectra, ESR, DSC/TGA, and specific-surface (BET) determination. The primary diamond grains are larger (15-16 nm) than in ordinary nanodiamond from RDX/TNT blends (ca. 5 nm) but smaller than in HFND from benzotrifuroxan (27 nm), with electron spins distributed in volume. HFND is much less hygroscopic and more prone to oxidation than ordinary nanodiamond. When heated in air up to 400ºC, HFND shown a drastic increase of oxygen/carbon ratio without an apparent loss of mass. The mechanism of hydrogen non-contamination (through segregation of detonation gases) and particle growth is discussed.

Keywords: detonation, hydrogen-free, nanodiamond, oxidation, particle size

1. Introduction

Different allotropic forms of nanocarbon [1] attract intense interest and find a widening variety of applications, due to their multifunctional properties. Thus, composites involving graphitic-type (sp^2-C) nanophases, such as carbon black [2], nanotubes [3-6] and 2D-carbon flakes [7] and are prospective for catalytic, optoelectronic, gas-sorption and ion-scavenging applications, thermally

*Corresponding author. E-mail address: batsanov@mail.ru (S. S. Batsanov)

reduced graphene for copolymer building blocks [8] and graphene quantum dots for photo-luminescence and supercapacitance devices [9]. On the other hand, nanodiamond (ND) particles (sp^3-C) [10, 11] which are now industrially produced [12] at low cost by detonation of high explosives, have actual and potential applications ranging from drug delivery to quantum computers, besides more conventional uses, such as abrasive materials. Another prospective area is 'neutron optics'. ND is the most efficient reflector of very cold neutrons (VCN) in their entire energy range, due to fortunate combination of physical parameters: the size of nanoparticles is comparable with the VCN wave length, they provide high neutronoptical potential and low neutron absorption [13-15]. The energy of a cold neutron can be further reduced on interaction with ultracold ND [13]. Thus the density of VCN can be increased by many orders of magnitude, with exciting methodical results. Unfortunately, ND usually contains up to 1% of hydrogen, most of which cannot be removed by degassing, thermal treatment, etc. Large inelastic scattering by ^{1}H makes it a most unwelcome impurity, causing large loss of neutrons and much devaluing ND as a neutron-optics material [15], while its isotopic replacement with deuterium is very difficult. Therefore it is highly desirable to prepare intrinsically hydrogen-free ND (HFND).

The formation of ND, both chemically and physically, is a far-from-equilibrium, multi-stage process of great complexity, still imperfectly understood [12, 16-21]. Indeed, the very appearance of condensed carbon is a challenge the canonical theory of the plane wave steady detonation process [22]. Two conditions are considered indispensable: the explosive having negative oxygen balance (*OB*), i.e. an excess of carbon over oxygen, and suitable thermodynamic parameters on the Chapman−Jouguet (CJ) plane [23-25], i.e. the surface where the reacting gases just reach sonic velocity as the chemical reaction (and energy release) is essentially complete. These parameters, temperature T_{CJ} and pressure P_{CJ}, depend on the detonation velocity W_d, hence on the composition, structure and porosity of the explosive. Industrially, ND is usually prepared by detonating RDX (hexogen, $C_3H_6N_6O_6$) blended in various proportions with trinitrotoluene (TNT, $C_7H_5N_3O_6$). Formation of ND requires T_{CJ} >3000 K and P_{CJ} > 30 GPa and begins with nucleation (near the CJ plane) of carbon nanoclusters from supersaturated carbon vapour. During the subsequent isentropic expansion of the detonation products, these clusters coagulate into nanodroplets of carbon, which crystallize and grow in the diamond structure, as at these conditions (3400–2900 K, 16.5–10 GPa) nanodiamond is thermodynamically more stable than graphite [17]. As the opposite is true at lower pressures, the products must be cooled rapidly to the temperature where thermodynamic

favourability of the diamond→graphite conversion is nullified by its high kinetic barrier. This is achieved by allowing the detonation gases to expand into large volume of a blast chamber and/or by surrounding the charge with a shell of ice or liquid water (the so-called 'wet method') which both reduces the temperature *and* extends the duration of high pressure. Then the post-explosion soot is treated by oxidizing acids ($HClO_4$, HNO_3/oleum, *aqua regis*, etc.) or by ozone to eliminate the graphitic phase.

This scheme has many caveats. *OB* is conventionally calculated assuming only H_2O, N_2 and CO_2 as gaseous products, but in fact the reaction is often incomplete and yields CO. It was therefore suggested [26] that the *OB* <0 condition is not enough and the carbon/oxygen atomic ratio must exceed 1, in which case pure RDX should not yield ND. Homogenous nucleation model fits awkwardly with highly non-homogenous nature of post-detonation media. On nanoscale, both the melting conditions and the equilibrium between graphite and diamond are different from those of the bulk phases (to which the conventional phase diagram refers!), but even for the latter the melting conditions of diamond are debatable. Carbon coagulation being exothermic, the droplets can become much hotter than the detonation products themselves; CJ plane is not easy to define for multistage reaction. The experimental studies, difficult due to extreme rapidity of the reactions, aimed primarily at increasing the yield of ND, and therefore paid relatively little attention to the fate of impurities. Thus, to our knowledge, there has been no inquiry whether the hydrogen contamination comes from the explosive(s), the coolant or even the oxidizing solution.

Recently, we prepared HFND by detonation of a hydrogen-free explosive, benzotrifuroxan (BTF, $C_6N_6O_6$) [27]. (Interestingly, Titov et al used the same explosive in 1993 [28] and probably obtained HFND without recognizing it, as neither elemental analysis nor chemical properties of the ND product were reported.) However, the synthesis of BTF [29] is expensive, and the yield of HFND from it is low (ca. 5%). Therefore in the present work we developed a technique of preparing HFND from cheap mass-produced explosives. In the process, we clarified some general aspects of ND synthesis and comprehensively characterized the physico-chemical properties of HFND, which differ substantially from those of ND prepared conventionally from RDX/TNT blends.

2. Experimental part

Commercial RDX was obtained from the *Altay* Federal Scientific-Industrial Centre (Biysk, Russia), BTF from the *Soyuz* Federal State Unitary Enterprise (Moscow Region, Russia), carbon black (particles size ca. 200 nm, elemental analysis: C, 97.51; N, 0.19; H, 0.35%) from the Technical

Carbon Co (Yaroslavl, Russia), synthetic μm-sized diamond powder from Euro Superabrasives Ltd (Darlington, UK).

Detonation experiments used a cylindrical explosive charge assembled of 10 pressed disks, 8.8 mm thick and 20.1 mm in diameter, enclosed in an ice shell and detonated in a nitrogen-filled steel chamber. The recovered soot was refluxed with concentrated perchloric acid to remove the graphitic component and then repeatedly refluxed with fresh portions of boiling de-ionized water until approximately neutral reaction, whereupon ND was precipitated from colloidal solutions by centrifugation (at 15,000 rpm) and dried in air at 200^{o}C until constant weight. The explosive charge consisted either of pure commercial RDX or of RDX doped with 5% of graphitic carbon black, yielding ND products **1** and **2**, respectively. BTF-derived HFND **3** [27] and ordinary ND **4** [30] were prepared as described earlier and purified identically to **1** and **2**. Teflon and (for centrifugation) nalgene vessels were used throughout, to exclude contamination by silica from glassware.

CHN analysis was carried out on a freshly calibrated Carlo Erba 1106 automatic analyzer [31]; samples were burnt under flow of oxygen at 1050 ºC (1800ºC at the moment of flash), the combustion products (N_2, CO_2, H_2O) were chromatographed in a flow of He gas. The X-ray diffraction patterns were recorded on a modernized DRON powder diffractometer (Cu-*K*α-radiation, λ= 154.18 pm). Grain sizes, τ, were calculated using Scherrer equation

$$\tau = \frac{K\lambda}{\beta cos\theta} \quad (1)$$

where K = 0.94 and β is the peak half-width in radians. The total particle sizes D were estimated from the observed specific surface area S and density ρ (hence V = 1/ρ), assuming spherical particle shapes, as

$$D = \frac{V}{S} = \frac{\pi D^3/6}{\pi D^2} = \frac{6}{\rho S} \quad (2)$$

Specific surfaces were measured on a Gemini VII 2390 V1.02t instrument (Micromeritics Instrument Co) by N_2 gas adsorption at 77.3 K, using an adaptive rate and static volumetric technique. Samples were dried and degassed at 200^{o}C, then kept under vacuum for 12 h before being weighed and analysed; the data were processed using Brunnauer-Emmett-Teller (BET) model. Densities of HFND powders were measured by liquid picnometry in toluene. ESR spectra were recorded using the State Standard Instrument in National Research Institute of Physical-Technical Measurements (Russia) with the signal modulation of 0.5 Gs. IR spectra were recorded on Perkin Elmer Spectrum One and Universal ATR Accessory instrument by the method of full internal

reflection. Raman spectra were recorded using a Horiba Jobin-Yvon LabRamHR, equipped with a 532 nm laser, and calibrated against Si line (520 cm^{-1}). DSC/TGA measurements were carried out using a NETZSCHSTA 409 PC/PG instrument, heating rate 10 K/min.

TEM and SAED experiments were performed on a JEOL 2100 F field emission gun instrument (microscope voltage 80 kV). The solution containing nanodiamond was sonicated and deposited on a holey carbon grid. Energy-dispersive X-ray spectra were recorded on an Oxford Instruments EDX spectrometer. EELS spectrum was recorded on Gatan Tridiem instrument, including spectrum imaging in scanning TEM (STEM) mode [32].

3. Results

3.1 Preparation of HFND

Our approach was based on comparison of the relevant parameters of explosives (Table 1). Note that in the RDX/TNT blend, commonly used in ND production, TNT is the major source of excess carbon, whereas RDX is needed to enhance the pressure. As the *OB*, detonation velocity and CJ pressure of pure RDX are all comparable to those of BTF (which is known to yield HFND), we used RDX to prepare HFND. It is well known that both the thermodynamic parameters and the products of detonation strongly depend on the porosity, i.e. the effective bulk density (ρ) of the explosive charge (the values in Table 1 refer to monolithic samples with the maximum density ρ_o). We calculated these dependences according to ref. 23 and found that an increase of ρ, i.e. a decrease of porosity, should lower T_{CJ} and rise the yield of solid soot (Fig. 1). Detonation of pure pressed RDX with ρ = 1.72 g cm^{-3} (94% of the monolithic ρ_o) yielded 7.5% of soot, from which 3% (relative to the initial charge mass) of HFND was isolated (product **1**). In view of the theory, we tried to increase the yield by doping RDX with 5% of graphitic carbon black and thereby increasing ρ to 1.76 g cm^{-3}. While this indeed boosted the yield of *soot* to 10%, the yield of HFND (product **2**) actually fell to 2%.

Table 1 Properties of explosives [24]

Explosive	BTF	RDX	TNT	RDX/TNT blend
Formula	$C_6N_6O_6$	$C_3H_6N_6O_6$	$C_7H_5N_3O_6$	$C_3H_6N_6O_6$ ·$C_7H_5N_3O_6$
OB, %	–14.0	–21.6	–74.0	–47.8
ρ_o, g cm^{-3}	1.90	1.83	1.65	1.70

W_d, km s^{-1}	8.62	8.85	6.95	7.75
T_{CJ}, K	4200	3300	3000	3150
P_{CJ}, GPa	34.9	33.8	19.0	27.3

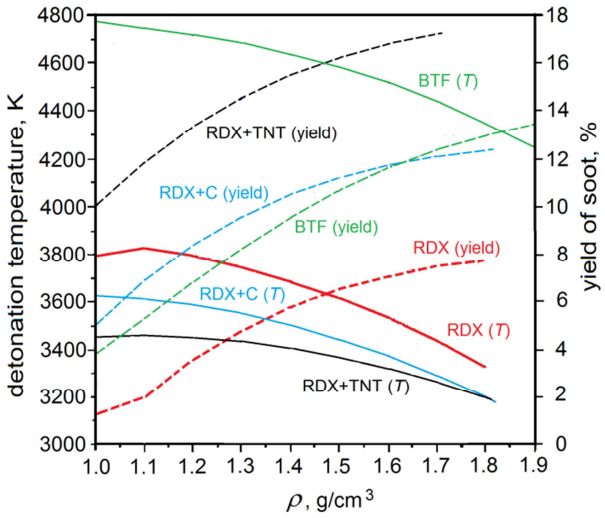

Figure 1. Detonation temperature, T_{CJ} (solid lines) and soot yield (dashed lines) as functions of density (ρ) of explosives

Table 2 Composition of fresh and air-oxidized ND

	T (ºC) and time of air exposure	C, %	N, %	H, %	O, % [d]
1	as prepared [a]	88.63	1.03	0	9.4
1	250 (2 days)	75.89	0.97	0	22.1
1	400 (3 days)	70.15	0.66	0	28.2
1	470 (2 hours) [b]	61.30	0.47	0	38.2
1	550 (2 hours) [c]	54.40	0.00	0	44.6
1	670 (2 hours)	39.1	0.00	0.25	60.6
1	25 (2 years)	63.97	0.75	0.33	33.0
2	as prepared [a]	80.92	1.16	0	16.9

2	250 (2 days)	78.28	1.05	0	19.7
2	300 (3 days)	77.47	0.96	0	20.4
2	400 (3 days)	77.29	0.72	0	21.0
2	25 (2 years)	60.49	0.78	0.19	37.5
3	as prepared[e, g]	86.7	2.6	0	10.7
3	as prepared [f, g]	84.0	2.3	0.12	12.6
4	as prepared	85.13	1.97	0.69	11.9
4	400 (3 days)	84.23	2.25	0.66	11.9
4	25 (2 years)	84.64	1.97	0.86	11.5

[a] average, for individual samples see Table S1; [b] mass loss 2.9%; [c] mass loss 19.5%; [d] balance, assuming 1% Fe; [e] from pressed BTF; [f] from BTF doped with 5% of carbon black; [g] ref. 27

3.2 Characterisation of HFND

The elemental analyses are presented in Table 2. Both **1** and **2** contained *ca.* 1% of nitrogen (an ubiquitous impurity in ND) and *ca*. 1% of iron originating from the walls of the blast chamber (which yielded 1.5% of non-combustible Fe_2O_3 residue) while carbon contents varied. The balance was presumably oxygen, which is always present in ND [12]. HFND samples **3**, obtained from pressed BTF with $\rho = 1.84$ g cm^{-3} or from loose BTF powder with $\rho = 0.88$ g cm^{-3} (Table 1), as well as those obtained earlier [21] from BTF with various additives, had similar carbon contents (81-91%), although their nitrogen contents varied widely, from 1.2 to 8.0%. EDS spectra of either **1** or **2** (Figure 2) show a prominent peak of C and admixtures of O, Fe and Si, the latter probably extracted by shock waves from Si-containing steel of the blast chamber [33].

The hydrogen content in **1** and **2,** as in **3**, was found to be nil within the experimental error. Admittedly, the latter amounts to 0.2% for this type of analyzers [31] and is substantial relative to the hydrogen content of ordinary ND. Nevertheless, the absence of hydrogen was reproducible for a variety of samples. Unfortunately, alternative methods for hydrogen determination (e.g. NMR spectroscopy [34]) cannot easily prove its *absence*, especially when the location and chemical bonding state of hydrogen is unclear (*vide infra*). Furthermore, ND is notoriously ill-suited for mass-spectroscopy, being non-volatile, difficult to ionize and prone to graphitization, although some

encouraging results have been obtained recently with diamond films, using industrial hydrogen analyzer and hydrogen extraction at high temperature [35].

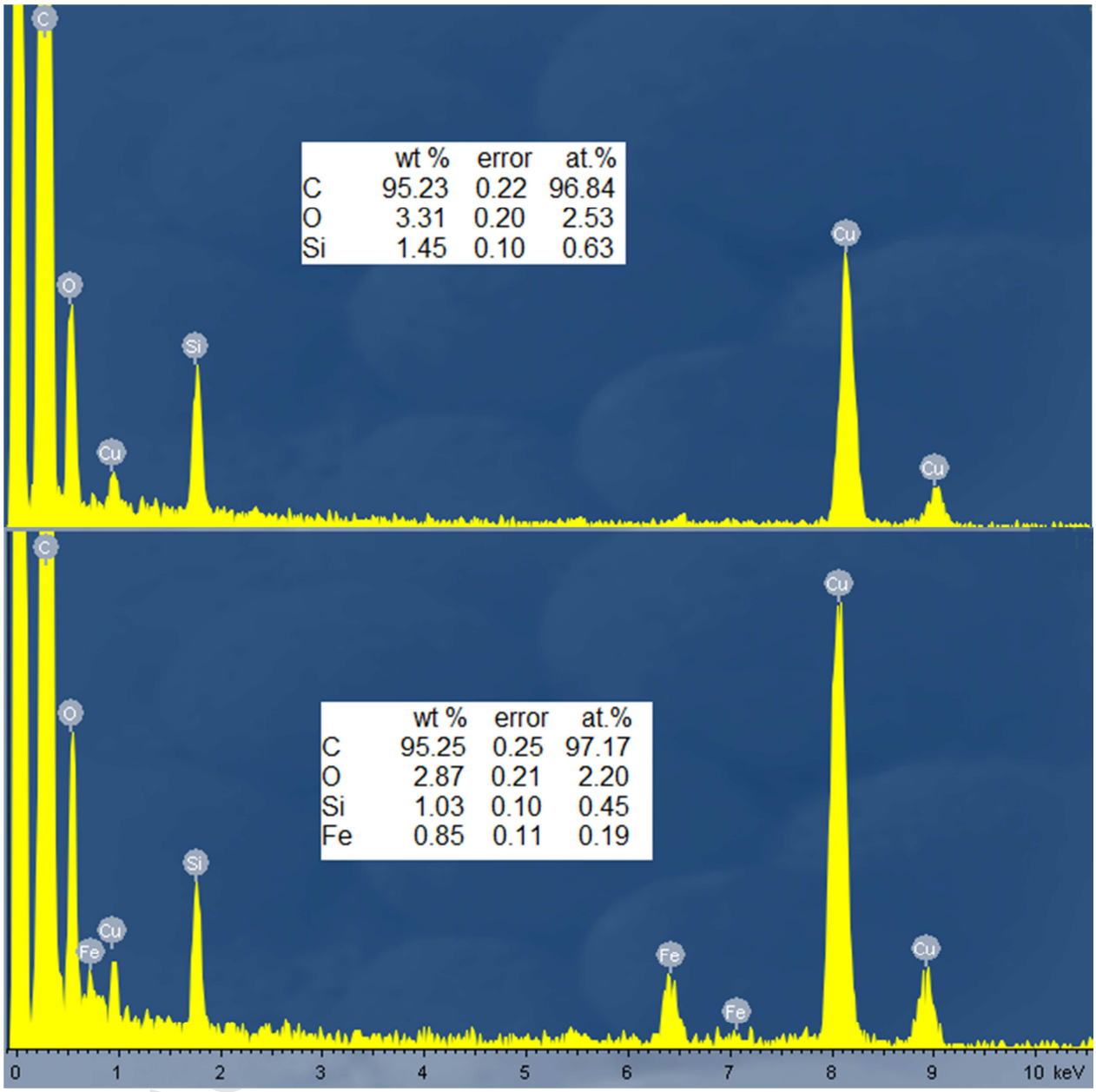

Figure 2. EDS spectra of **1** (top) and **2 (**bottom). Copper signals come from the grid and carbon (partly) from the holey

Table 3 Physical properties of ND

Characteristics	HFND **1**	HFND **2**	HFND **3** [a]	ND **4**

Parent explosive	RDX	RDX+carbon	powder BTF	RDX/TNT blend
Formula	$C_6N_6O_6$	$C_3H_6N_6O_6$	$C_7H_5N_3O_6$	$C_3H_6N_6O_6 \cdot C_7H_5N_3O_6$
τ, nm	15.2(8)	15.8(11)	26.9[b]	5.4(4)
S, m^2g^{-1}	45.4	51.3	37.1	316
ρ, g cm^{-3}	3.345	3.425	3.10	3.35
D, nm	39.5	34.2	52.2	5.9
ESR: Δ, Gs	7.05	6.30	7.03	8.50
$C_p \times 10^{-17}$	5.36		5.92	8.00
$C_s \times 10^{-19}$/g	6.4, 3.3[c]	7.9, 6.6[c]	6.9	8.0, 8.0[c]

[a] from ref. 7; [b] cf. 20-40 nm from TEM [27]; [c] after heating for 2 h at 150°C

X-ray diffraction patterns of **1** and **2** (see SI, Figures S1, S2 and Tables S1, S2) showed the reflections (111), (220) and (311) of cubic diamond (a = 0.3569 nm) with usual relative intensities of 100:18:9. A few additional weak reflections were present, alongside a broad feature of amorphous/turbostratic carbon, ranging from 2θ≈18 to 30° [36]. The reflection with 2θ≈12.6° (d ≈ 7.2 Å) probably belongs to graphite oxide [37] which resulted from incomplete oxidation of graphitic phase during purification. According to the literature, the position of this reflection may vary widely, from 2θ≈10 to over 12°, depending on the oxidation conditions [37]. It is noteworthy, however, that the major reflection of fullerene C_{60} occurs in the same range [38]. The peak at 2θ ≈ 26.6° is evidently the (002) reflection of residual non-oxidized h-graphite, that at 2θ≈24.8° can be attributed to 'disordered' graphite which forms, e.g., during ball-milling and has wider inter-layer separations, further increasing as the particle size diminishes [36]. The reflections at 2θ≈35.5° and 33.2° to the β-form of carbon nitride C_3N_4 [39]. The latter phase is known to form under high-energy ball-milling, hence may also be generated under detonation shock; the nitrogen may originate from the N_2 with which the explosive chamber was filled, as well as from the explosive itself. The non-diamond peaks are much less prominent in product **2** than in **1**; they were also observed in BTF-derived **3** (Figure S3). As shown in Table 3, the mean size τ of diamond nanoparticles (i.e. of the regions of coherent X-ray scattering) in **1** and **2** are much smaller than in HFND **3** obtained from BTF but larger than in ordinary ND (**4**). High-resolution TEM (Figure 3) broadly confirmed these sizes and showed that crystalline grains coexist with amorphous regions,

especially in **1**, whereas **2** shows higher degree of crystallinity. Selected-area electron diffraction (SAED, Figure 4) showed discrete reflections from nanocrystals overlapping with diffuse rings, the Bragg angles of both characteristic of cubic diamond. A few sharp reflections, however, are not attributable to diamond and suggest different nanocrystalline phase(s), in agreement with X-ray diffraction. EELS spectra (Figure 5) of crystalline regions were typical of ND, while amorphous regions contained larger amount of sp^2 carbon.

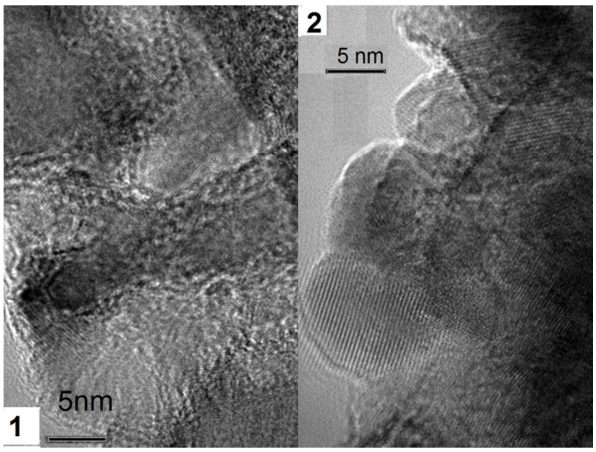

Figure 3.High-resolution TEM images of **1** and **2.**

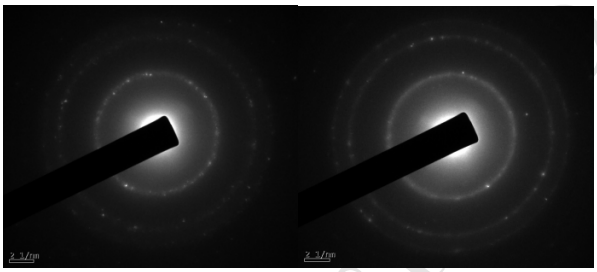

Figure 4. SAED patterns of HFND samples **1** (left) and **2** (right)

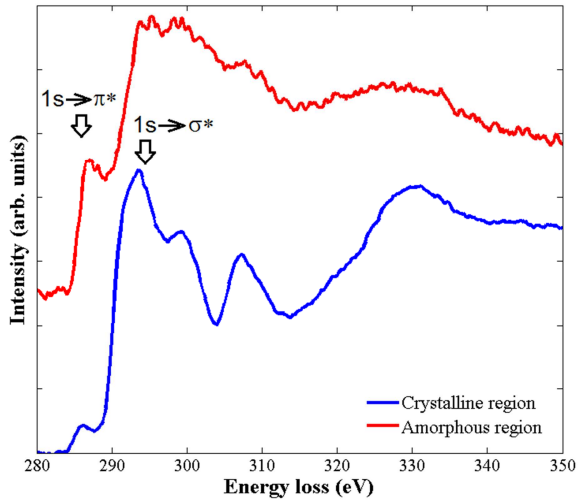

Figure 5. EELS spectra of **1**

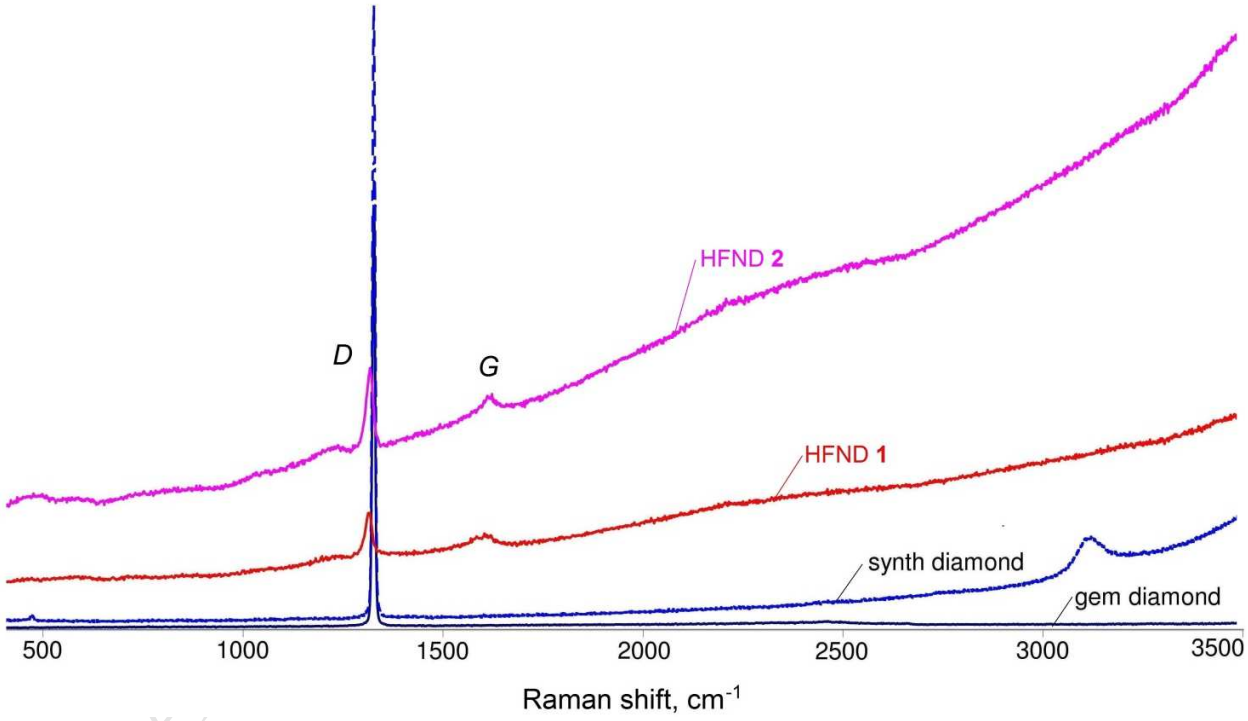

Figure 6. Raman spectra of HFND **1** and **2**, compared to natural gem-grade diamond and synthetic polycrystalline diamond. *D* – diamond peak, *G* – graphitic G-band.

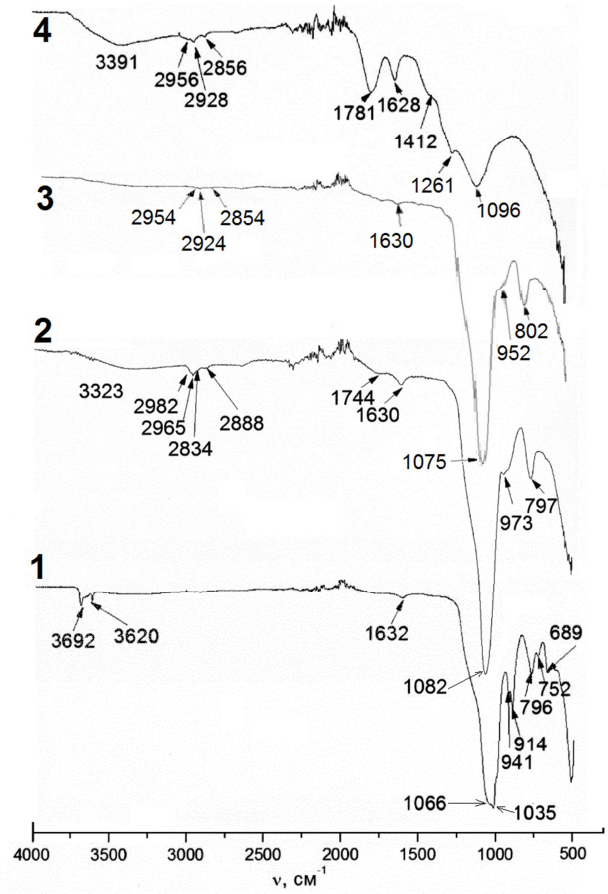

Fig. 7. IR spectra of nanodiamond samples **1**–**4.**

Raman spectroscopy of ND is complicated by its strong luminescence. The first-order Raman spectrum of monocrystalline natural (gem-grade) diamond consists of a single narrow peak around 1331 cm^{-1} and that of polycrystalline (micron-sized) synthetic diamond powder is very similar (Figure 6), both **1** and **2** show the diamond peak slightly downshifted (to ca. 1318 cm^{-1}) and broadened. These changes indicate weakened C–C bonding and defect-rich structures in the nanoparticles and have been observed in ordinary ND as well [40]. An additional broader peak around 1600 cm^{-1} (with the maximum at 1620 cm^{-1}) in **1** and **2** is likewise commonly observed in ordinary ND and resembles G-band of graphite (1590 cm^{-1}). However, HFND lacks the broad and rather intense feature at 1500-1800 cm^{-1}, typical for ordinary ND and attributed to adsorbed molecules and surface functional groups, especially O–H and C=O [19]. Likewise, IR spectra of HFND (**1**-**3**) do not show the ν(O–H) bands typical for ordinary ND (Figure 7), in agreement with

much lower hydrophilicity of HFND. The ESR spectra of **1-4** (Table 3) have similar shapes, with *g*= 2.0021 ± 0.0001.

The measured specific surface areas *S* suggest the total ('mechanical') particle sizes *D* more than twice the τ in **1** or **2**, but only slightly larger than τ in **4**. Interestingly, product **3** from BTF *powder* is similar in this respect to **1** and **2** (*D*>>τ, see Table 3) while **3** obtained from *pressed* BTF (at much lower temperature) shows *D*=28.9 nm very close to τ=27.5 nm.

3.3 Oxidation of HFND

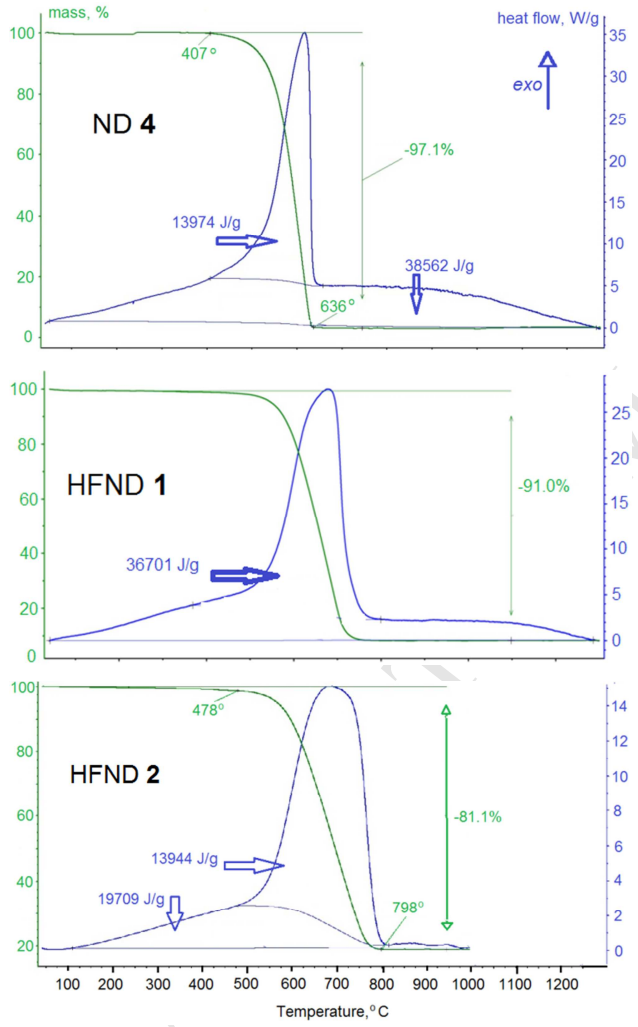

Fig. 8. TGA/DSC for nanodiamond samples **1, 2**and**4** (oxidation in air)

DSC/TGA study of **1**, **2** and **4** on heating in air (Figure 8), showed the combustion (i.e. an exothermic peak simultaneous with a rapid weight loss) between 500 and 800 ºC for **1** and **2**, and between ca. 400 and 650 ºC for **4**. This well-known stage is preceded, however, by an exothermic

process *without any apparent weight loss*. To explore it, we subjected samples of **1**, **2** and **4** to protracted heating in air at various constant temperatures (Table 2), as distinct to fast increase of temperature during DSC/TGA study. Subsequent elemental analyses revealed a striking change of composition, i.e. an increase of oxygen/carbon ratio, within a constant weight. At 470 and 550 ºC, oxygen content in **1** increased further, albeit accompanied by a weight loss. The changes were less drastic in **2** than in **1**, although it must be taken into account that **2** contained more oxygen to begin with. The samples of **1** and **2** which were long exposed to atmospheric air at room temperature, showed a similar oxidation (Table 3). On the contrary, ordinary ND (**4**) showed little change, either on heating to 400 ºC (i.e. just under the onset of combustion) or during long storage in air. In either case, long-exposure samples acquired small amounts of hydrogen, probably through hydrolysis of the surface layer by atmospheric moisture.

X-ray diffraction of these samples oxidized at 290, 390, 490 and 550 ºC (see SI) is still dominated by the diamond reflections which show no broadening. On heating to 290 and 390°C, the reflections of all admixtures remain virtually unchanged, on further heating they gradually diminish with a corresponding increase of the amorphous carbon halo. Finally, **1** oxidized at 670 ºC shows mainly this halo, as well as sharp peaks of h-graphite and carbon nitride and much weakened and broadened reflections (111) and (220) of HFND. This picture agrees with earlier observations that oxidation of diamond is accompanied by its graphitization [41].

We also recorded ESR spectra after heating the samples for 2 hours at 150ºC. For **1** and **2**, C_s decreased roughly in proportion to the decreasing carbon content (see above), while remaining unchanged for **4**, which does not oxidize under these conditions. This, again, suggests a fairly uniform distribution of spins in the volume of the particles, and probably their diamond cores as well as the outer shells.

4. Discussion

To understand the results, three distinct but interconnected questions must be answered: (i) why ND is not contaminated with hydrogen in the present case – or why it usually is, (ii) why HFND forms bigger particles than ordinary ND and (iii) why the agglomeration modes of HFND and ND are different. As a matter of fact, hydrogen can originate only from the explosive itself: note that we detonated both BTF [27] and RDX (the present work) in ice shells and purified the products by $HClO_4$ in water, without contaminating them. BTF is just hydrogen-free, but RDX contains more hydrogen than TNT, relative both to carbon *and* to oxygen. H has lower electronegativity than C

and therefore must oxidize first, so it may seem surprising that RDX yields HFND whereas RDX/TNT blends do not. The simplest answer is that *OB* of RDX being less negative than that of TNT, growing ND particles loose competition for hydrogen to a more oxidative medium, as the formation of H_2O is thermodynamically preferable to C–H bonding. For more sophisticated explanation, let us consider decomposition of TNT and RDX in detail. According to theoretical simulations [20], a TNT molecule first loses its substituents. Carbon clusters begin to form at this stage and (as proven by ^{14}C labeling experiments [16]) include disproportionally large amount of carbon atoms from the methyl groups. The latter are not entirely decomposed in the process [16] and so can carry H atoms into ND particles. The aromatic ring, due to its high resonance energy, survives longer and its carbon goes largely into graphitic soot.

An RDX molecule already contains N–N fragments, therefore its decomposition begins with rapid (10 ps) ejection of N_2 molecules, followed by slightly slower (30 ps) production of H_2O and much slower (900 ps) release of CO and CO_2 simultaneous with growth of carbon and carbon-oxygen clusters [21]. Such different rates may help an effective segregation of the post-explosion gas mixture into spatially-separated components, the mechanism of which we described elsewhere [42]. At the later stage, this can produce carbon-rich (but impurity-poor!) regions from which the hydrogen-free nanoparticles can grow. Incidentally, this helps to answer question (ii). Note that detonation-produced ND is unique among manufactured nanomaterials in having a rather narrow size distribution of primary particles (typically, $\tau \approx 5$ nm), which so far defied a comprehensive explanation and largely frustrated attempts to alter this size. Thus, prolonging the duration of high pressure by a 20-fold increase of a TNT/RDX charge, barely increased particle sizes twofold, from 3-4 to 6-8 nm [18]. By contrast, BTF easily gave a 5-fold increase, to 27 nm (Table 2), which was initially attributed to higher T_{CJ} of BTF (Table 1) [28], but in the present work we obtained particles of 15-16 nm from RDX, i.e. without any substantial increase of T_{CJ}. The succession can be rationalised thus. Growth of a particle, whether liquid or solid, requires sufficient number of collisions between *identical* molecules/atoms, hence simply having fewer components in the gas facilitates growth. In **1** and **2**, this is due only to spatial segregation of components, while for BTF, the detonation gas also has fewer components to begin with, as the absence of hydrogen excludes H_2O, CH_4, etc.

A complementary explanation is that hydrogen itself hinders the growth of ordinary ND crystals, being (by virtue of its monovalence) the most efficient terminating agent for dangling bonds on the

ND surface, which otherwise could link to further carbon atoms. Indeed, there is experimental evidence [43] that such hindering actually occurs: with increasing hydrogen concentration, minimum conditions for diamond synthesis increase steeply, while an excess of TiH_2 suppresses diamond growth altogether. Without this inhibition, HFND particles grow bigger, hence have relatively fewer surface atoms and fewer sites for hydrogen, which in ND is mostly located at the surface (as shown by NMR [27]), although it can also participate in internal defects [44, 45].

Different agglomeration modes can be explained thus. The surface of ordinary ND is terminated by hydrogen atoms and/or hydrogen-containing groups, is hygroscopic and covered by interfacial water [46, 47], all of which makes the particles easier to disaggregate. In contrast, HFND particles are not hygroscopic [28] and (as revealed by TEM) are more tightly agglomerated, either directly or through outer shells of non-diamond carbon, which also may evolve because the diamond surface is less efficiently terminated and instead is stabilized by amorphization and/or graphitization.

For RDX/TNT blends, the yield of ND depends linearly on the proportion of explosives [17]. Extrapolation of this dependence to pure RDX suggests the yield of 4-8%, in broad agreement with our results.

The availability of larger particles provides new evidence for the long-standing controversy about the origin of ESR signals in ND. The early naïve view identifying these signals with dangling bonds on the surface has been disproven by NMR spectra more consistent with electron spins distributed within the disordered shell, 0.4 to 1 nm from the surface [48]. Furthermore, paramagnetism of ND is not affected substantially by the method of preparation [49] and purification used, or even by chemical modification of the surface[50]; this also suggests that paramagnetic centres are located in the interior. It has even been argued that an entire ND particle can be regarded as a giant molecular radical [49]. For ordinary ND, it is difficult to distinguish between surface and volume effects, precisely because the particle size and hence the surface-to-volume ratio always vary in an unusually (for nanomaterials) narrow range. Now we found that the spin concentrations C_s relative to mass are very similar for **1**-**4**, notwithstanding the difference in particles sizes, specific areas and chemical nature of their surfaces. This strongly supports the view that spins are widely distributed in the volume of the particles.

The most unusual feature of HFND is its thermal behaviour: although it burns at higher temperature than ordinary ND, HFND is much more prone to *pre*-combustion oxidation than ND. From the particles size alone, the opposite could be expected: oxidation of a solid requires an

expenditure of atomization energy, which is lower for smaller nanoparticles [51]. Instead, one should conclude that the surface of ordinary ND is thermodynamically stabilized by C–H termination, which rids the surface of dangling bonds. This is impossible in HFND and leaves it prone to surface oxidation, the heat of which facilitates the diamond to graphite phase transition. In principle, it is possible to envisage an oxidation process whereby removal of surface carbon atoms in the form of CO_2 (or CO with its subsequent oxidation in the gas phase) is compensated by binding of O atoms to the same surface. However, it would require some highly unusual mechanism to achieve a precise compensation of mass in this process, so that four carbon atoms are replaced exactly by three oxygen ones – the more so because neither ND nor HFND have stoichiometric composition themselves – nor does graphene oxide, an obvious example of nanocarbon oxidation. The following, entirely hypothetical, scheme can illustrate that such substitution is not impossible in principle. Let us consider the oxidation of a {111} face, which is, alongside {100}, the most common for smaller nanoparticles of diamond [52] and also the one preferentially oxidized [53, 54]. This face can be described as a puckered hexagonal layer, half of atoms in which have outward-directed dangling bonds. In the virtual absence of hydrogen, the latter cannot be terminated by OH or COOH groups, whereas an –O–bridge between two unsaturated C atoms is geometrically impossible. However, such atoms can be connected by a –C(=O)O–bridge (Figure 9) [55]. Thus, removing a layer of 2*N* carbon atoms and terminating the resulting *N* dangling bonds with *N*/2 bridging CO_2 groups, amounts to replacing three carbon with two oxygen atoms. On an {100} face, or an edge between two {111} faces, where dicoordinate carbon atoms are present, these can be replaced by equal number of O atoms. Whilst the combination of these two *may* amount to a 4C/3O substitution, there are numerous sources of perturbations, from crystal defects to possible presence of carbonyl (C=O) groups or –C(=O)OC(=O)– bridges. Note also that, contrary to common perception, oxygen in ND can be present in the interior of the particle and not exclusively on the surface [56]. In any case, this issue is extremely interesting and deserves further investigation, which is currently in progress.

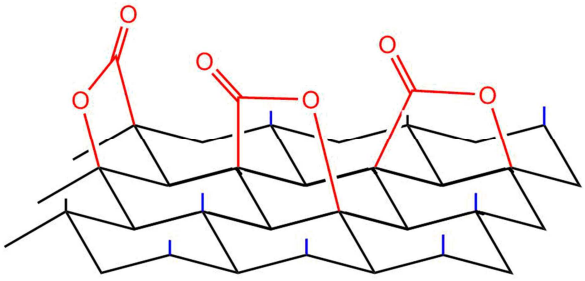

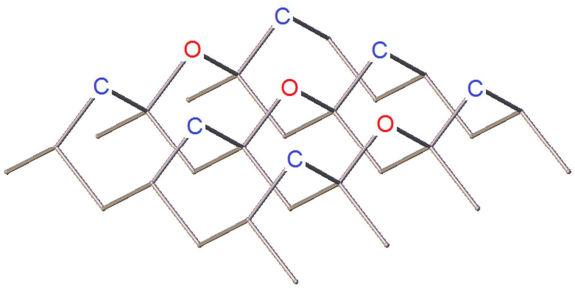

Fig. 9. A hypothetical scheme for HFND surface oxidation. Top: face {111} showing dangling bonds (blue) and their bridging by CO_2 groups (red). Bottom: face {100} showing dicoordinate atoms (blue) and their partial replacement by oxygen

An important corollary is: one should not presume that constant weight guarantees constant chemical identity – until this is proven analytically! It may be necessary to reassess the common routine of drying ND after wet purification *to constant weight* at 150-250 ºC or even at higher temperatures. The risks of skipping elemental analysis are manifest in the history of the Dalan diamond synthesis [57], a technique intermediate between detonation ND production (where the source of carbon is the explosive itself) and the conventional diamond synthesis, where the explosive is only a source of pressure applied to graphite or carbon black. Dalan uses a mixture of RDX with graphite (19%) or carbon black (12.5%) and thus resembles our preparation of HFND **2**. With RDX/graphite blend, Dalan also gives enlarged ND grains, of 10-20 nm. Thus it is not impossible that HFND was obtained – but not recognised, as the product (intended for industrial uses) was only crudely purified and neither its chemical nor phase composition was reported.

5. Conclusions and outlook

We have demonstrated that preparation of HFND from RDX is a practicable process; it can be viable even with the current low yield, given the immense possibilities which an efficient neutron-optics material can open in various fields of materials science. Our further work (currently in progress) is aimed at raising the yield of HFND by optimizing the preparation protocol, as well as exploring the relation (which is predicted theoretically) between the particle size of HFND and its efficiency as a reflector of neutrons, and how the latter is affected by various impurities other than hydrogen.

We also found that HFND has larger particle sizes than ordinary ND but similar concentration of electron spins, proving that the latter are *not* confined to the surface. HFND is less hygroscopic than

ND but is oxidized easier and, amazingly, the O/C ratio increases while the mass remains constant on heating up to 400 ºC, which implies a near-quantitative replacement of 4 carbon with 3 oxygen atoms. The mechanism of this oxidation, unprecedented in both materials chemistry and organic chemistry, requires further investigation which is currently planned. A practical corollary is that the common routine of drying ND to constant weight may not guarantee constant chemical composition.

Another currently ongoing study in our laboratory concerns aqueous colloids of various types of ND (including HFND), both as an important stage in ND preparation [1, 12, 46] and because of their unique physical properties [30, 47] and peculiar biological behavior [58].

Acknowledgement

The authors thank Dr. I. V. Kolesnik and Dr. T. B. Shatalova (Chemistry Department, Moscow State University) for help with IR and DSC experiments, respectively, and Ms E. D. Strel'tsova (Institute of Organic Chemistry RAS, Moscow) for elemental analysis.

Supplementary data

X-ray powder diffraction data, TEM images, electron diffraction images, energy-dispersive X-ray spectra, and EELS spectra, can be found at http//….

References

[1] O.A. Shenderova, V.V. Zhirnov, D.W. Brenner, Carbon nanostructures, Crit. Rev. Solid State Mater. Sci. 27 (2002) 227−356.

[2] K. R. Reddy, B. C. Sin, K. S. Ryu, J. Noh, Y. Lee, In situself-organization of carbon black–polyaniline composites from nanospheres to nanorods. Synth. Met. 159 (2009) 1934–1939.

[3] K. R. Reddy, B. C. Sin, K. S. Ryu, J.-C. Kim, H. Chung, Y. Lee, Conducting polymer functionalized multi-walled carbon nanotubes with noble metal nanoparticles. Synth. Met. 159 (2009) 595–603.

[4] K. R. Reddy, B. C. Sin, C. H. Yoo, W. Park, K. S. Ryu, J.-S. Lee, D. Sohn, Y. Lee, A new one-step synthesis method for coating multi-walled carbon nanotubes with cuprous oxide nanoparticles. Scripta Materialia 58 (2008) 1010–1013.

[5] K. R. Reddy, K.-P. Lee, A. I. Gopalan, M. S. Kim, A. M. Showkat, Y. C. Nho, Synthesis of metal (Fe or Pd)/alloy (Fe–Pd)-nanoparticles embedded multiwall carbon nanotube/sulfonated polyaniline composites by γ-irradiation. J. Polymer Sci. A: Polymer Chem. 44 (2006) 3355-3364.

[6] M. U. Khan, K. R. Reddy, T. Snguanwongchai, E. Haque, V. G. Gomes, Polymer brush synthesis on surface modified carbon nanotubes via in situ emulsion polymerization. Colloid Polym Sci 294 (2016) 1599–1610.

[7] S. Venkateswarlu, D. Lee, M. Yoon, Bioinspired 2D-carbon flakes and Fe_3O_4 nanoparticles composite for arsenite removal. ACS Appl. Mater. Interfaces 8 (2016) 23876−23885.

[8] D. R. Son, A. V. Raghu, K. R. Reddy, H. M. Jeong, Compatibility of thermally reduced graphene with polyesters. J. Macromol. Sci. Part B: Phys. 55 (2016) 1099–1110.

[9] M. Hassan, E. Haque, K. R. Reddy, A. I. Minett, J. Chen, V. G. Gomes, Edge-enriched graphene quantum dots for enhanced photo-luminescence and supercapacitance. Nanoscale 6 (2014) 11988−11994.

[10] O. A. Williams (Ed.).Nanodiamond. RSC Nanoscience and Nanotechnology: Cambridge, 2014.

[11] A. Vul', O. Shenderova (Eds). Detonation nanodiamonds – science and applications. Pan Stanford Publishing: Singapore, 2014.

[12] V.Yu. Dolmatov, Detonation-synthesis nanodiamonds: synthesis, structure, properties and applications, Russ. Chem. Rev. 76 (2007) 339−360.

[13] V.V. Nesvizhevsky, Interaction of neutrons with nanoparticles, Physics Atomic Nuclei 65 (2002) 400−408.

[14] V.V. Nesvizhevsky, G. Pignol, K.V. Protasov, Nanoparticles as a possible moderator for an ultra cold neutron source, Int. J. Nanoscience 6 (2007) 485−500.

[15] A. R. Krylov, E. V. Lychagin, A. Yu. Muzychka, V. V. Nesvizhevsky, G. V. Nekhaev, A. V. Strelkov, A. S. Ivanov, Study of bound hydrogen in powders of diamond nanoparticles. Crystallogr. Rep. 56 (2011) 1186–1191.

[16] E. V. Mironov, E. A. Petrov, A. Ya. Korets, From analysis of the structure of ultrafine diamond to the problem of its formation kinetics. Combust. Expl. Shock Waves 40 (2004) 473–476.

[17] V. V. Danilenko, Specific features of synthesis of detonation nanodiamonds. Combust. Expl. Shock Waves 41 (2005) 577–588.

[18] V. V. Danilenko, Coagulation of carbon clusters in a detonation wave. Combust. Expl. Shock Waves 53 (2017) 93–102.

[19] V. N. Mochalin, O. Shenderova, D. Ho, Y. Gogotsi, The properties and applications of nanodiamonds. Nature Nanotechnology 7 (2012) 11-23.

[20] D. Furman, R. Kosloff, F. Dubnikova, S. V. Zybin, W.A. Goddard III, N. Rom, B. Hirshberg, T.Y. Zeiri, Decomposition of condensed phase energetic materials: interplay between uni- and bimolecular mechanisms. J. Amer. Chem. Soc. 136 (2014) 4192–4200.

[21] Y. Li, R. K. Kalia, A. Nakano, P. Vashishta, Multistage reaction pathways in detonating RDX. AIP Conference Proceedings 1793 (2017) 030007.

[22] S. Bastea, Nanocarbon condensation in detonation. Sci. Rep. 7 (2017) 42151.

[23] R. Meyer, J. Köhler, A. Homburg, Explosives, 6th Edition;Wiley-VCH:Weinheim, 2007.

[24] N.A. Imhovik, Thermodynamics and thermochemistry of explosive and detonation processes, in: 'Physics of Explosion' (vol.1, p. 125), L. P. Orlenko, Ed., Physmatlit: Moscow, 2002 (in Russian).

[25] A. Dolgoborodov, M. Brazhnikov, M. Makhov, S. Gubin, I. Maklashova, Detonation performance of high-dense BTF charges, J. Phys. Conf. Ser. 500 (2014) 052010.

[26] B.P. Tolochko, V.M. Titov, A.P. Chernyshev, K.A. Ten, E.R. Pruuel, I.L. Zhogin, P.I. Zubkov, N.Z. Lyakhov, L.A. Lukyanchikov, M.A. Sheromov, Physical-chemical model of processes at detonation synthesis of nanodiamond. Diamond Relat. Mater. 16 (2007) 2014−2017.

[27] S.S. Batsanov, A.N. Osavchuk, S.P. Naumov, A.E. Efimov, B.G. Mendis, D.C. Apperley, A.S. Batsanov, Synthesis and properties of hydrogen-free detonation diamond. Propell. Explos. Pyrotech. 40 (2015) 39−45.

[28] I. Yu. Mal'kov, L.I. Filatov, V.M. Titov, B.V. Litvinov, A.L. Chuvilin, T.S. Teslenko, Formation of diamond from the liquid-phase of carbon. Combust. Explos. Shock Waves 29 (1993) 542−544.

[29] E.A. Chugunova, R.E. Timasheva, E.M. Gibadullina, A.R. Burilov, R. Goumont, First synthesis of benzotrifuroxan at low temperature. Propell. Explos. Pyrotech. 37 (2012) 390-392.

[30] S.S. Batsanov, S.M. Gavrilkin, A.S. Batsanov, K.B. Poyarkov, I.I. Kulakova, D.W. Johnson, B.G. Mendis, Giant dielectric permittivity of detonation-produced nanodiamond is caused by water, J. Mater. Chem. 22 (2012) 11166−11172.

[31] W.J. Swindall, D. T. Burns, Improvements to the CHN performance of a Carlo-Erba 1106 elemental analyser. Fresenius Z. Anal. Chem. 331 (1988) 730−734.

[32] C. Jeanguillaume, C. Colliex, Spectrum-image: the next step in EELS digital acquisition a processing, Ultramicroscopy 28 (1989) 252−257.

[33] S. S. Batsanov, A. S. Batsanov, Shock synthesis of single crystals. Propell. Explos. Pyrotech. 38 (2012) 169−171.

[34] D.C. Apperley, R.K. Harris, P. Hodgkinson, Solid state NMR, Basic principles & practice. Momentum Press: New York, 2012.

[35] A.M. Polyanskiy, V.A. Polyanskiy, Yu.A. Yakovlev, N.A. Feoktistov, V.G. Golubev, A.Ya. Vul', Determining the content and binding energy of hydrogen in diamond films. Tech. Phys. Lett. 41 (2015) 540−542.

[36] Z.Q. Li, C.J. Lu, Z.P. Xia, Y. Zhou, Z. Luo, X-ray diffraction patterns of graphite and turbostratic carbon. Carbon, 45 (2007) 1686−1695.

[37] T.N. Blanton, D. Majumdar, X-ray diffraction characterization of polymer intercalated graphite oxide, Powder Diffraction, 27 (2012) 104−107.

[38] B.M. Ginzburg, Sh. Tuĭchiev, S. Kh. Tabarov, A.A. Shepelevskiĭ, L.A. Shibaev, X-ray diffraction analysis of C_{60} fullerene powder and fullerene soot, Tech. Phys. 50 (2005) 1458−1461.

[39] Y. Fahmy, T.D. Shen, D.A. Tucker, R.L. Spontak, C.C. Koch, Possible evidence for the stabilization of β-carbon nitride by high-energy ball milling. J. Mater. Res. 14 (1999) 2488−2499.

[40] J. Cebik, J. K. McDonough, F. Peerally, R. Medrano, I. Neitzel, Y. Gogotsi, S. Osswald, Raman spectroscopy study of the nanodiamond-to-carbon onion transformation. Nanotechnology, 24 (2013) 205703.

[41] T. Evans, Changes produced by high temperature treatment of diamond, in: Field, J. D. (Ed.).The properties of diamond. Acad. Press: London, 1979, pp. 403−425.

[42] S.S. Batsanov, Thermodynamic reasons for delamination of molecular mixtures under pressure and detonation synthesis of diamond, Russ. J. Phys. Chem. 83 (2009) 1419−1421.

[43] Z.F. Zhang, X.P. Jia, S.S. Sun, X.B. Liu, Y. Li, B.M. Yan, H.A. Ma, Effects of hydrogen impurity on diamond crystal growth process. Int. J. Refractory Metals & Hard Materials 38 (2013) 111−117.

[44] J.P. Goss, Theory of hydrogen in diamond. J. Phys. Cond. Matter, 15 (2003) R551−R580.

[45] P. Briddon, R. Jones, G.M.S. Lister, Hydrogen in diamond. J. Phys. C Solid State Phys. 21 (1988) L1027−L1031.

[46] M. Ozawa, M. Inaguma, M. Takahashi, F. Kataoka, A. Kruger, E. Ōsawa, Preparation and behavior of brownish, clear nanodiamond colloids, Adv. Mater. 19 (2007) 1201−1206.

[47] S.S. Batsanov, E.V. Lesnikov, D.A. Dan'kin, D.M. Balakhanov, Water shells of diamond nanoparticles in colloidal solutions, Appl. Phys. Lett. 104 (2014) 133105.

[48] X.-W. Fang, J.-D. Mao, E.M. Levin, K. Schmidt-Rohr, Nonaromatic core-shell structure of nanodiamond from solid-state NMR spectroscopy, J. Am. Chem. Soc. 131 (2009) 1426–1435.

[49] P.I. Belobrov, S.K. Gordeev, É.A. Petrakovskaya, O.V. Falaleev, Paramagnetic properties of nanodiamond, Doklady Physics 46 (2001) 459–462.

[50] I.I. Kulakova, V.V. Korol'kov, R.Yu. Yakovlev, G.V. Lisichkin, The structure of chemically modified detonation-synthesized nanodiamond particles, Nanotechnologies in Russia 5 (2010) 474–485.

[51] S.S. Batsanov, A.S. Batsanov, Introduction to Structural Chemistry; Springer: Dordrecht, 2012.

[52] N.A. Feoktistov, S.A. Grudinkin, V.G. Golubev, M.A. Baranov, K.V. Bogdanov, S.A. Kukushkin, Evolution of the morphology of diamond particles and mechanism of their growth, Phys. Solid State 57 (2015) 2184–2190.

[53] C.Q. Sun, H. Xie, W. Zhang, H. Ye, P. Hing, Preferential oxidation of diamond {111}, J. Phys. D, Appl. Phys. 33 (2000) 2196–2199.

[54] J.Y. Howe, L.E. Jones, D.W. Coffey, The evolution of microstructure of CVD diamond by oxidation, Carbon 38 (2000) 929–941.

[55] B.J.M. Etzold, I. Neitzel, M. Kett, F. Strobl, V.N. Mochalin, Yu. Gogotsi, Layer-by-layer oxidation for decreasing the size of detonation nanodiamond, Chem. Mater.26 (2014) 3479–3484.

[56] T. Jiang, K. Xu, FTIR study of ultradispersed diamond powder synthesised by explosive detonation. Carbon, 33 (1995) 1663−1671.

[57] V.F. Tatsii, A.V. Bochko, Structure and properties of Dalan detonation diamonds. Comb. Expl. Shock Waves, 45 (2009) 95−103.

[58] S.S. Batsanov, D.L. Guriev, S.M. Gavrilkin, K.A. Hamilton, K. Lindsey, B.G. Mendis, H.J. Riggs, A.S. Batsanov, On the nature of fibres grown from nanodiamond colloids. Mater. Chem. Phys. 173 (2016) 325−332.

TOC

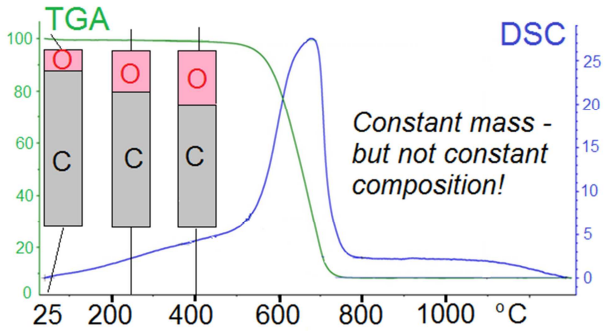

Novel synthesis and properties of hydrogen-free detonation nanodiamond

Stepan S. Batsanov, Alexander N. Osavchuk, Stepan P. Naumov, Sergey M. Gavrilkin, Anatoly S. Leskov, Budhika G. Mendis, Andrew Beeby and Andrei S. Batsanov

Highlights

- Detonating pure RDX yields hydrogen-free nanodiamond prospective for neutron optics
- Larger particles than ordinary nanodiamond
- Enigmatic oxidation without apparent weight loss